
QuIRK : Quantum-Inspired Re-uploading KAN

Vinayak Sharma
Arizona State University, Tempe
Vinayak.Sharma@asu.edu

Ashish Padhy
National Institute of Technology, Rourkela
ashishpadhy1729@gmail.com

Lord Sen
National Institute of Technology, Rourkela
123cs0226@nitrkl.ac.in

Vijay Jagdish Karanjkar
Arizona State University, Tempe
vkaranj@asu.edu

Sourav Behera
National Institute of Technology, Rourkela
souravdipu2002@gmail.com

Shyamapada Mukherjee
National Institute of Technology, Rourkela
mukherjees@nitrkl.ac.in

Aviral Shrivastava
Arizona State University, Tempe
Aviral.Shrivastava@asu.edu

Abstract

Kolmogorov-Arnold Networks or KANs have shown the ability to outperform classical Deep Neural Networks, while using far fewer trainable parameters for regression problems on scientific domains. Even more powerful has been their interpretability due to their structure being composed of univariate B-Spline functions. This enables us to derive closed-form equations from trained KANs for a wide range of problems. This paper introduces a quantum-inspired variant of the KAN based on Quantum Data Re-uploading (DR) models. The Quantum-Inspired Re-uploading KAN or QuIRK model replaces B-Splines with single-qubit DR models as the univariate function approximator, allowing them to match or outperform traditional KANs while using even fewer parameters. This is especially apparent in the case of periodic functions. Additionally, since the model utilizes only single-qubit circuits, it remains classically tractable to simulate with straightforward GPU acceleration. Finally, we also demonstrate that QuIRK retains the interpretability advantages and the ability to produce closed-form solutions.

1 Introduction

Kolmogorov-Arnold Networks (KANs) [1] were introduced as a class of networks based on the Kolmogorov-Arnold Representation Theorem (KART) [2, 3] and promised to be more efficient in smaller function learning tasks than Deep Neural Networks (DNNs). According to KART, a multivariate continuous function f on a bounded domain can be written as a finite composition of univariate functions.

$$f(x_1, x_2, \dots, x_n) = \sum_{q=1}^{2n+1} \Phi_q \left(\sum_{p=1}^n \phi_{q,p}(x_p) \right) \quad (1)$$

Where $f : [0, 1]^n \rightarrow \mathbb{R}$ defines the outer function and $\phi_{q,p} : [0, 1] \rightarrow \mathbb{R}$ and $\Phi_q : \mathbb{R} \rightarrow \mathbb{R}$ define the inner functions used for approximation. A major challenge when applying this theorem to machine learning (ML) is that the 1-D functions $\phi_{q,p}$ might be non-smooth or even fractal. However, Liu et al. argued that in the average case most functions in science

are smooth and have sparse composite structure. This allows us to use smooth functions, in their case B-Splines, as the basis to create a network that can scale to arbitrary breadth and depths.

The choice of B-Splines as the basis for KANs has proven to be effective, but, they are not the only functions we may use in order to construct KAN models. In principle, we could use any univariate universal function approximator as the basis for a KAN model. However, for practical purposes we would like these univariate functions to be expressive, compact and easy to compute. Data Re-Uploading (DR) circuits [4] are a class of QML algorithms that fit these characteristics and hence can form a promising new basis for KAN models.

Quantum Machine Learning (QML), is a field of machine learning which seeks to exploit the special properties of quantum circuits in order to create new more efficient ML models. Pérez-Salinas et al., introduced the Data Re-Uploading Classifier, which was proven to be a Universal Classifier based on the *Universal Approximation Theorem* [5] of DNNs (Eqn. 2).

$$h(\vec{x}) = \sum_{i=1}^N \alpha_i \cdot \sigma(\vec{w}_i \cdot \vec{x} + b_i) \quad ; \alpha_i, b_i \in \mathbb{R} \quad (2)$$

Specifically the authors used a corollary which stated that σ could be a non-constant finite linear combination of periodic functions. This allowed DR models to create universal function approximators using rotational quantum gates. Critically, this proof also makes DR models eligible univariate functions to utilize as building blocks for KANs.

We utilize the universal approximation functionality of DR models in order to construct a new variant of the KAN model called QuIRKs. QuIRK incorporate DR models in place of B-Splines while maintaining the same scalability in depths and breadth structure as KANs. Due to the inherent higher dimensionality of qubits compared to real-valued univariate functions, DR models are far more expressively compact. This increased dimensionality is due to two main factors - (1) The vectorized nature of qubits caused by superposition. (2) The complex-valued nature of qubit states. This allows our DR based QuIRK to use fewer trainable parameters and smaller model sizes when compared to KANs for a similar level of accuracy as shown experimentally in the results (??) section.

Another important aspect of QuIRKs is that they can be easily accelerated on GPUs. We refer to our model as ‘*Quantum Inspired*’ because, although we utilize a QML model, the structure of our network does not require any quantum computers for training or inference. Due to the lack of entanglement, all our circuits are factorizable into single qubit circuits and can be computed using 2×2 matrix multiplications (matmuls) on simulators. These matmul operations are far more optimized for modern GPUs as compared to B-Splines used by KANs. This allows for better computational scaling as compared to KANs. Additionally, the use of these quantum inspired mathematical structures allows us to leverage the expanded feature space of quantum systems. It is important to note that current backpropagation implementations and optimizers struggle with complex numbers and hence we leverage the capabilities of quantum simulators in this domain to train our models.

Therefore, the main features of the QuIRK model can be summarized as follows:

1. Data re-uploading based scalable network architecture,
2. Parameter efficient KAN model leveraging the higher dimensionality of quantum systems,
3. Computationally scalable due to simple 2×2 matrix multiplication based implementation.

2 Related Work

The idea of a Quantum Kolmogorov-Arnold Network (QKAN) was first proposed by Ivashkov et al. [6]. In their work they used linear combination of Chebyshev polynomials, through QSVT [7], as learnable activation functions in place of B-splines. However, the focus of their work was creating a theoretical framework to implement KAN on quantum computer and their number of qubits scale linearly with inputs while gates scale quadratically with layers leading to an exponential increase in computational cost. We propose a novel architecture that combines the benefits of the Kolmogorov-Arnold Network (KAN) and the Data Re-Uploading (DR) Classifier to create a scalable, quantum-inspired, classical architecture, while still using a predetermined number of qubits making it NISQ compatible.

Kolmogorov-Arnold Network (KAN) [1] are networks based on the Kolmogorov-Arnold Representation Theorem (KART) [2]. As opposed to Multi-Layer Perceptrons (MLPs) which are composed of units with fixed non-linear functions of weighted sums of inputs, KAN units are sums of trainable univariate functions (or activations). In the original work these activations were B-Splines [8]. The original KART was defined for 2 layers, Liu et al. [1] generalized the KART to multiple layers which allowed them to construct scalable network architectures.

Our work explores replacing B-Splines used by Liu and Wang et al. with a universal classifier similar to the work by Shen et al. [9]. While they explored using DNNs as trainable activation functions, we propose using Data Re-Uploading (DR) classifiers [4] as the activation functions. These models have the same approximation guarantees via the UAT as DNNs while being significantly cheaper to compute by exploiting the larger feature space of quantum systems.

Data Re-uploading classifiers (DR) [4] are a class of QML models that exploit hybrid classical-quantum computation to circumvent the no-cloning theorem. Pérez-Salinas et al. [4] proposed an analogue to classical DNNs which learn multiple functions in a single variable to approximate a target function. The DR circuit therefore ‘re-uploads’ the input Data at the beginning of each layer, allowing the model to learn multiple functions in a single variable. This approach allowed the authors to establish approximation guarantees for DR classifiers using the Universal Approximation Theorem (UAT) [5].

A key advantage of this approach is the fact that DR models are universal function approximators in a single variable, which allows us to use them as extremely efficient activation functions in the KAN architecture. A single qubit can be simulated very efficiently on a classical computer via 2×2 matrix multiplication, thus making our architecture extremely scalable.

3 QuIRK Architecture

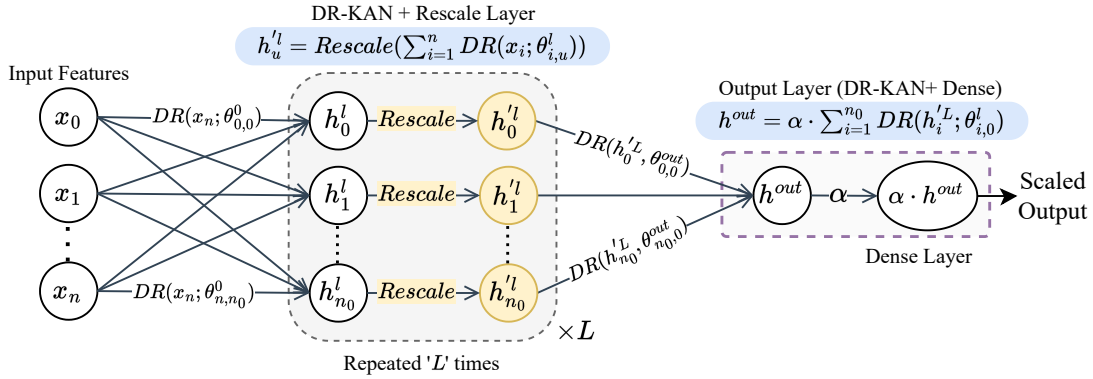


Figure 1: QuIRK Macro architecture. Each incoming edge to a QuIRK layer is a single qubit DR circuit. The output of each hidden QuIRK layer (h_u^l) is then rescaled to the range $[0, \pi]$ creating node h_u^l . The output of the network is a QuIRK layer with a single unit followed by an *optional* dense layer which scales the output to the desired range.

QuIRK largely inherits the structure of classical KAN models. As such, it is composed by an Inner and Outer function as shown in Eqn. 1. The outer function (Φ) refers to the operation of summation of the DR circuit outputs in each layer. The inner functions (ϕ) are DR circuits which learn univariate functions. Additionally, we introduce a ‘Rescale’ layer between QuIRK layers in order to account for the domain and range of DR circuits. As shown in Fig. 1, we can create deeper models by stacking blocks of QuIRK layer and rescale layers. Finally, a classical dense layer with a single unit is optionally appended to scale the output data ($[-1, 1] \rightarrow \mathbb{R}$). We can therefore distill the QuIRK model into 4 main components:

1. **QuIRK layers**, which consist of multiple QuIRK units.
2. **QuIRK units**, which each consist of sums of DR circuits over the input data.
3. **Rescale layers**, which rescale the output of each QuIRK unit from $\mathbb{R} \rightarrow [0, \pi]$.
4. **Classical Dense layers**, which can optionally be appended to the output of the QuIRK layer to scale the output $[-1, 1] \rightarrow \mathbb{R}$ if required.

3.1 QuIRK layers

QuIRK Layers are composed of units which sum over the expectation values of DR circuits. Formally, we can define the output of the i^{th} unit of the layer ‘l’ as:

$$h_i^{(l)} = \sum_{i=1}^{|I|} DR(x_i; \theta_{i,u}^l) \text{ for } x_i \in I \quad (3)$$

Where, I is the set of inputs to the layer, $DR(x_i; \theta_{i,u}^l)$ the DR circuit better the i^{th} unit of the previous layer and u^{th} unit of the current layer with parameters $\theta_{i,u}^l$, and ‘ x ’ is the input to the QuIRK layer.

We know that the output of the DR circuit is the expectation value of the final quantum state. This state is created by applying a series of parameterized unitary gates which can be combined to into a single unitary ($U(x_i; \theta_i^{(l)})$) that is applied to the initial state $|0\rangle$. The expectation value of this final state w.r.t the computational basis is represented by the operation $\langle \psi \rangle$, where $\psi = U(x_i; \theta_i^{(l)}) |0\rangle$. Therefore, we can unpack the DR layer in Equation. 3 as -

$$h_i^{(l)} = \sum_{i=1}^{|I|} \langle U(x_i; \theta_i^{(l)}) |0\rangle \rangle \text{ for } x_i \in I \quad (4)$$

A lot of the power of these layers can be associated to the representative power of DR models. While in the single qubit setting they may be limited when trying to approximate multi-variate functions, they excel in the univariate scenario. In principle DR models map the 1-D data onto a higher dimensional Hilbert space, a space with 2 complex dimensions in the single qubit space, where they learn a linear map. This linear map is then projected back to the 1-D space. As shown by Boser et al. [10], linear maps in higher dimensional spaces can approximate non-linear functions in lower dimensional spaces. This means that the QuIRK units can learn arbitrarily complex univariate functions. This idea is further explored in the next section.

3.2 DR Activations

Data Re-Uploading models exploit the ability to ‘re-upload’ data in hybrid classical-quantum models in order to create universal function approximators. They accomplish via multiple DR-layers each consisting of a data encoding function $\phi(x)$ followed by a trainable unitary $U(\theta_i)$ as shown in Fig. 2. Each layer can therefore be consolidated into a single unitary $U^{(i)}(x, \theta^{(i)})$ which is a new function of the input ‘ x ’. The final state of each DR node can therefore be described as:

$$U(x; \theta) |0\rangle = \left(\prod_{i=0}^L U^{(L-i)}(x, \theta^{(L-i)}) \right) |0\rangle \quad (5)$$

The choice of $U(\theta_i)$ is not fixed and can be constructed using an arbitrary combination of single qubit parameterized gates (ex. R_Y, R_X and R_Z). This choice determines the number of trainable parameters used by DR unit and the expressivity of the DR layers. In general $U(\theta_i) = R_Z(\theta_i[0])R_Y(\theta_i[1])R_Z(\theta_i[2])$, which is proven to be the universal SU2 group. Therefore, using DR models introduces 2 hyperparameters to the QuIRK model - (1). The number of DR layers in each node, and (2). The choice of $U(\theta_i)$.

In our implementation, $\phi(x) = R_Y(x)$ and $U(\theta_i) = R_Z(\theta_i[0])R_X(\theta_i[1])$. Therefore, we use only 2 parameters per DR layer.

3.2.1 Multi Qubit Extensions

The QuIRK model can also be scaled to use multiple qubits per edge in order to learn richer features at the cost of increased computation and more training parameters. The use of multiple qubits per edge also allows us to utilize entanglement. As pointed out by Pérez-Salinas et al. [4], entanglement can significantly reduce the number of trainable parameters required to approximate a function. This increased parameter efficiency comes at the risk of an exponential blow up in the size of our matrix multiplications and hence computation. However, due to the overall the structure of QuIRK, the DR units only need to learn univariate functions. Therefore, in practice the number of qubits remains

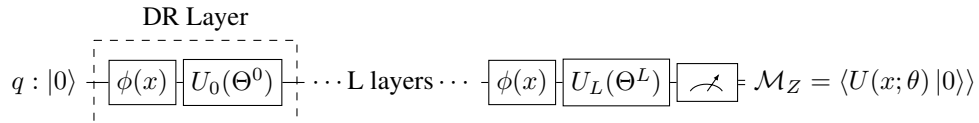


Figure 2: Single qubit Data Re-Uploading circuit with ‘ L ’ layers. Each layer consists of a data encoding function $\phi(x)$ following by a trainable unitary $U(\Theta^i)$. The final measurement is a function of the input ‘ x ’ and the trainable parameters ‘ $\theta = \{\Theta^i \mid \forall i \in [0, L]\}$ ’. Each activation is composed of multiple DR layers.

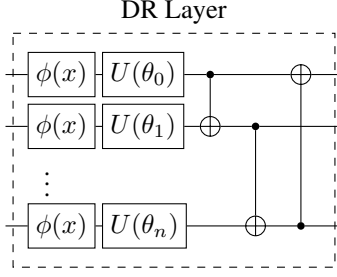


Figure 3: Multi qubit (n) Data Re-Uploading layer. The layer consists of a set of trainable gates, an input embedding function and an entanglement pattern.

below 5 which can be computed via 32×32 matrices. This is still a reasonable computational cost for most modern computers.

The structure of a multi qubit DR models is outlined in Fig. 3. The layer consists of a set of trainable gates, an input embedding function and an entanglement pattern. Each qubit in encoded with the same data point, therefore even with multiple qubits, we are still learning a univariate function. The entanglement pattern is used to create a richer feature space as well as have our parallelly learned functions exchange information. The entanglement pattern is not fixed and can be chosen based on the problem at hand.

The multi-qubit QuIRK model therefore introduces 2 additional hyperparameters - (1). The number of qubits per edge, and (2). The entanglement pattern between qubits.

3.2.2 DR circuit Domain and Range

When using DR models, we have to keep 2 main limitations in mind and design our model around them. The first is that the output of each DR circuit is limited to the range $[-1, 1]$. The summation of multiple DR models in a unit therefore expands the range to $[-n, n]$, where ' n ' is the number of DR models in the unit. This plays into the 2nd limitation - the input to our DR models must be in the range $[0, \pi]$. This is due to the periodic nature of the gates used for data encoding, where data shifted by 2π maps to the same quantum state. These limitations can be addressed by using the 'rescale' layer as discussed in Section 3.3.

3.3 Rescale Layer

The use of DR circuits introduces constraints on the input and output ranges of our units. DR circuits encode data using Pauli rotational gates, which are periodic functions and the output for these circuits is a expectation value in the computational basis.

While we can technically have unbounded inputs to a Pauli rotational gate, the periodicity will create an issue where unique data points will map to the same quantum state. As an example consider 2 data points x, y such that $x = y + 4\pi$. Using the R_Y gate to encode the data starting from the $|0\rangle$ state will yield the states $|\phi(x)\rangle = \cos(x/2)|0\rangle + \sin(x/2)|1\rangle$ and $|\phi(y)\rangle = \cos(y/2)|0\rangle + \sin(y/2)|1\rangle$ respectively. Applying the relationship between x and y , we can see that $|\phi(y)\rangle = \cos(x/2 + 2\pi)|0\rangle + \sin(x/2 + 2\pi)|1\rangle = |\phi(x)\rangle$. As we can see, the two data points map to the same quantum state. Additionally, even if the values are within the period, the symmetric nature of sin and cosine functions can create cases where the feature map of two otherwise distinct data points have the same magnitude but differ only by sign. To avoid this issue we need to scale down the values to the range $[0, \pi]$.

Expectation values of quantum states are bounded between $[-1, 1]$. Therefore, the output of each QuIRK unit is bounded to $[-|I|, |I|]$ where ' $|I|$ ' is the number of incoming edges. This can create issues when the output of the QuIRK layer is used as input to the next layer due to the input domain of DR circuits. To address this, we introduce a 'Rescale' layer to scale our layer outputs to the domain required for the next layer. The output of the Rescale layer is given by:

$$\text{Rescale}(x_i) = \frac{x_i + (1 - b)}{2 \times |I|} \times \pi \quad (6)$$

As described in Eqn. 6, the Rescale layer divides each unit output by the upper bound ensuring a value between $[-1, 1]$. b is a boolean parameter which is set to 1 when bias is added the output of the DR-KAN, otherwise it is set to 0 and by

adding $1 - b$ to this and dividing by 2 we shift the range to $[0, 1]$. Finally, we multiply by π to ensure the input to the next layer is in the range $[0, \pi]$ (i.e. the range of unique values for the Pauli rotational gates).

3.4 Implementation Optimizations

QuIRK has been implemented using pennylane [11] and Tensorflow [12]. However, we have implemented a number of optimizations to improve the performance and scaling of our model. We employ the following strategies in order to create a practical and scalable model:

1. **Parallel Circuit Execution:** As we are using simulators with single qubits, we can efficiently run multiple circuits at a time.
2. **Tensor Network Simulations:** When running multiple batches of data across our parallel circuits, we can efficiently accelerate the execution via tensor network simulations. Nvidia’s cuTensorNet allows us to run these circuits on GPUs as well.
3. **Dynamic Circuit Creation:** We create our circuits dynamically on model instantiation based on input data sizes.

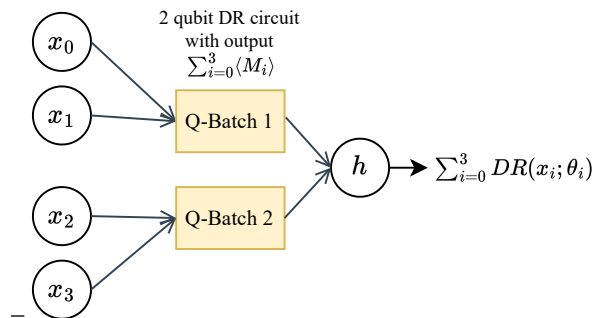


Figure 4: Q-batch execution for 4 dimensional data when ‘max_qubits’=2. The data is split into 2 batches and 2 circuits are run in parallel.

3.4.1 Parallel Circuit Execution

While pennylane already supports batching data when using the ‘backprop’ or ‘adjoint’ differentiation methods on simulators, that method is limited to batching input data rather than running multiple circuits with different weights as well. In order to achieve parallel execution with different weights we tested 2 separate approaches - (1). Q-batch execution and (2). Threaded Circuit execution.

In Q-batch execution, we define a ‘max_qubits’ parameter which determines the size of our circuit. We then batch our data into batches of size ‘max_qubits’ and run a single circuit with ‘max_qubits’ number of qubits. The circuit is run $C = \frac{N}{mq}$ times or ‘C’ circuits are run simultaneously, where N is the size of our input and mq is the max_qubits parameter.

While this method is effective, we have found that overhead in instantiation of these structures presents a bottleneck and as such our overall model runs fastest when using 5 qubits.

3.4.2 Tensor Network execution

Markov and Shi [13] showed that we can simulate quantum circuits with T gates and tree-width d (maximum number of qubits entangled together) in $T^{O(1)}e^{O(d)}$ time. As we are running single qubit networks in parallel, we have no entanglement and hence $d=1$. Therefore, we can simulate our circuits in $T^{O(1)}$ time, which is linear in the number of gates.

Exploitation of tensor network circuits and our unentangled networks allows us to efficiently scale to extremely large (< 30) qubit networks even on CPU.s. As shown in Fig. 5, we can run a QuIRK network with 100 dimensional input, a single QuIRK layer with 2 units and a dense layer using a 50-qubit circuit in under 10s on CPU.

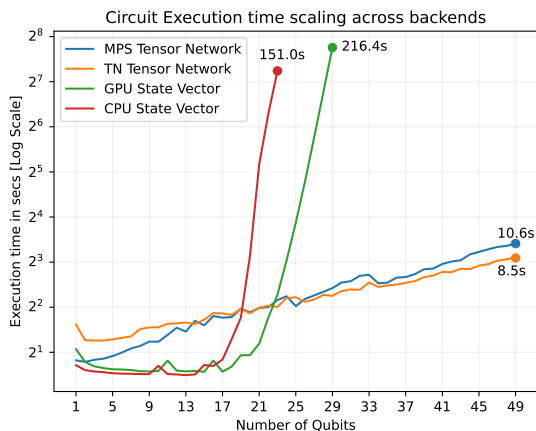


Figure 5: Runtime scaling of with increasing number of qubits across different backends using batch 8- 100 dim data on a 32-thread CPU and A6000 GPU. Tensor Network simulations greatly outperform the state-vector simulator for larger qubit counts but are worse for smaller qubit counts.

3.4.3 Dynamic Circuit Creation

Finally, we dynamically create our circuits based on the amount of data required in order to further reduce overhead. This is most relevant when our input data size is not fully divisible by mq . In this case, we can dynamically create a smaller circuit with the required number of qubits and add it to the computational graph. This allows us to run our model without any padding or wasted computation and limit the matrix dimensions.

4 Results

4.1 Experiments:

All experiments were run using PennyLane[11] and Tensorflow [12]. The system used for the experiments was a single NVIDIA RTX 4080 SUPER GPU and a Ryzen 7 7700X CPU with 32Gb of RAM.

4.2 Accuracy of QuIRK :

QuIRK model are able to showcase strong performance on regression tasks similar to KANs. As seen in table 1, QuIRK models show RMSE values 10^{-2} on most tasks. We can also see that QuIRK outperforms the vanilla KAN model on multiple equations such as I.6.2. This can be attributed to the superior performance of DR models as compared to B-Splines as a univariate function approximator.

4.3 Parameter Efficiency of QuIRK :

QuIRK models are able to fit functions using even fewer parameters than classical KANs while maintaining a comparable RMSE loss value. This can be attributed to the efficiency of DR models over B-Splines in fitting complex functions.

Table 1: QuIRK vs Classical KAN on RMSE and Parameter count on Feynman dataset [**Best in Bold**]

Equation	QuIRK (Ours)		QuIRK Pruned		Classical KAN		Classical KAN Pruned	
	Loss	# Params	Loss	# Params	Loss	# Params	Loss	# Params
I.6.2	8.40×10^{-3}	36	5.95×10^{-2}	24	3.90×10^{-1}	136	1.51×10^0	56
I.15.3x	1.30×10^{-2}	36	1.84×10^{-2}	24	5.14×10^{-1}	80	6.48×10^{-1}	56
I.26.2	7.07×10^{-2}	60	2.81×10^{-2}	40	4.20×10^{-3}	136	1.71×10^{-1}	56
III.9.52	3.06×10^{-2}	102	4.97×10^{-2}	62	2.20×10^{-4}	342	8.93×10^{-2}	72
I.44.4	3.74×10^{-2}	48	3.61×10^{-2}	24	4.63×10^{-2}	156	6.26×10^{-1}	56

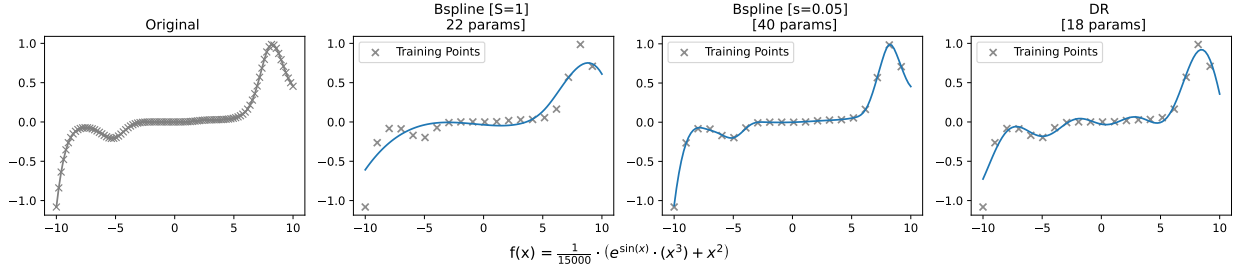


Figure 6: Parameter efficiency and function fitting capabilities of B-Splines vs Data Re-Uploading models. We compare against 2 B-Spline models with smoothness 1 and 0.05 resp. It is clear from the image that our DR circuit performs much better than the S=1 B-Spline and is slightly worse than the S=0.05 B-Spline.

Data Re-Uploading models learn global functions. In contrast, B-Splines learn functions in a piece wise manner and approximate these pieces using basis curves (degree 3 in the case of KANs). This difference can yield significant differences in the parameter efficiency of DR models and B-Splines.

As we can see in Fig. 6, the DR circuit is able to fit the function $\frac{1}{15000} (e^{\sin(x)} \cdot x^3 + x^2)$ using only 16 parameters. In comparison, even using 22 parameters B-Splines are not able to fit the function and only at 46 parameters do we see a good approximation. A larger set of comparisons can be found in Figure. A.1.

The increased efficiency of QuIRK units translates to smaller more efficient models that are able to achieve similar performance to classical KANs. This is evident in Table 1 where we see that QuIRK models are able to achieve similar RMSE values to classical KANs while using significantly fewer parameters.

4.4 Interpretability of QuIRK :

QuIRK models maintain the interpretability advantages of KANs. Due to still being composed of univariate functions, we can still analyze the outputs of each unit in the network. As seen in Fig. 7, we can fit the outputs of each DR unit to simple polynomials and then analyze these polynomials to construct a simplified output function. This allows us to derive closed form equations from trained QuIRK models similar to KANs.

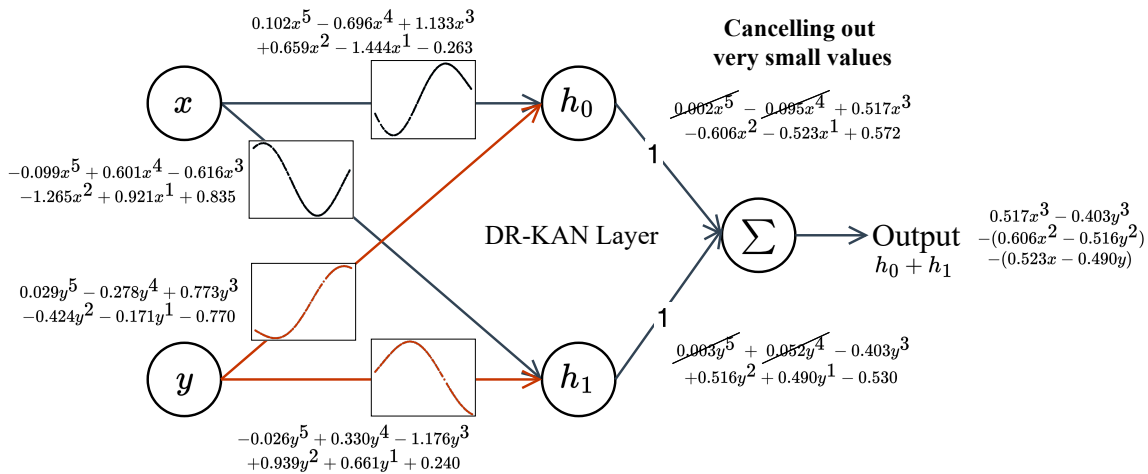


Figure 7: A single layer , 2 unit QuIRK with a simple sum on the output approximating the function $f(x, y) = x^2 - y^2$. We can see that the outputs of the DR units can be fit to 1-D polynomials. We can then analyze the polynomials to construct a simplified output.

5 Conclusion

In this paper we have presented QuIRK as an analogous and an efficient alternative to classical KANs. QuIRK uses batches of single qubit DR models as univariate function approximators as opposed to B-splines. Due to the efficiency of single qubit DRs, the learnable activation functions could be represented in much fewer parameters as compared to B-splines. Our experiments show that DR-KAN can achieve loss values similar to KANs with much fewer parameter counts A.1. DR-KAN also outperforms standalone DR models which is conclusive from table A.2.

References

- [1] Ziming Liu, Yixuan Wang, Sachin Vaidya, Fabian Ruehle, James Halverson, Marin Soljačić, Thomas Y. Hou, and Max Tegmark. Kan: Kolmogorov-arnold networks, 2024. URL <https://arxiv.org/abs/2404.19756>.
- [2] Vladimir I Arnold. On the representation of functions of several variables as a superposition of functions of a smaller number of variables. *Collected works: Representations of functions, celestial mechanics and KAM theory, 1957–1965*, pages 25–46, 2009.
- [3] Andrei Nikolaevich Kolmogorov. On the representation of continuous functions of many variables by superposition of continuous functions of one variable and addition. In *Doklady Akademii Nauk*, volume 114, pages 953–956. Russian Academy of Sciences, 1957.
- [4] Adrián Pérez-Salinas, Alba Cervera-Liarta, Elies Gil-Fuster, and José I. Latorre. Data re-uploading for a universal quantum classifier. *Quantum*, 4:226, February 2020. ISSN 2521-327X. doi: 10.22331/q-2020-02-06-226. URL <http://dx.doi.org/10.22331/q-2020-02-06-226>.
- [5] Kurt Hornik, Maxwell Stinchcombe, and Halbert White. Multilayer feedforward networks are universal approximators. *Neural networks*, 2(5):359–366, 1989.
- [6] Petr Ivashkov, Po-Wei Huang, Kelvin Koor, Lirandë Pira, and Patrick Rebstrost. Qkan: Quantum kolmogorov-arnold networks, 2024. URL <https://arxiv.org/abs/2410.04435>.
- [7] András Gilyén, Yuan Su, Guang Hao Low, and Nathan Wiebe. Quantum singular value transformation and beyond: exponential improvements for quantum matrix arithmetics. In *Proceedings of the 51st Annual ACM SIGACT Symposium on Theory of Computing, STOC 2019*, page 193–204, New York, NY, USA, 2019. Association for Computing Machinery. ISBN 9781450367059. doi: 10.1145/3313276.3316366. URL <https://doi.org/10.1145/3313276.3316366>.
- [8] Haskell B Curry and Isaac J Schoenberg. On spline distributions and their limits-the polya distribution functions. In *Bulletin of the American Mathematical Society*, volume 53, pages 1114–1114. AMER MATHEMATICAL SOC 201 CHARLES ST, PROVIDENCE, RI 02940-2213, 1947.
- [9] Zuwei Shen, Haizhao Yang, and Shijun Zhang. Neural network architecture beyond width and depth, 2023. URL <https://arxiv.org/abs/2205.09459>.
- [10] Bernhard E Boser, Isabelle M Guyon, and Vladimir N Vapnik. A training algorithm for optimal margin classifiers. In *Proceedings of the fifth annual workshop on Computational learning theory*, pages 144–152, 1992.
- [11] Ali Asadi, Amintor Dusko, Chae-Yeun Park, Vincent Michaud-Rioux, Isidor Schoch, Shuli Shu, Trevor Vincent, and Lee James O’Riordan. Hybrid quantum programming with pennylane lightning on hpc platforms, 2024. URL <https://arxiv.org/abs/2403.02512>.
- [12] Martín Abadi, Paul Barham, Jianmin Chen, Zhifeng Chen, Andy Davis, Jeffrey Dean, Matthieu Devin, Sanjay Ghemawat, Geoffrey Irving, Michael Isard, Manjunath Kudlur, Josh Levenberg, Rajat Monga, Sherry Moore, Derek G. Murray, Benoit Steiner, Paul Tucker, Vijay Vasudevan, Pete Warden, Martin Wicke, Yuan Yu, and Xiaoqiang Zheng. Tensorflow: A system for large-scale machine learning, 2016. URL <https://arxiv.org/abs/1605.08695>.
- [13] Igor L. Markov and Yaoyun Shi. Simulating quantum computation by contracting tensor networks. *SIAM Journal on Computing*, 38(3):963–981, January 2008. ISSN 1095-7111. doi: 10.1137/050644756. URL <http://dx.doi.org/10.1137/050644756>.

A Appendix / Supplemental Material

We include additional figures and tables to provide further insight into our experiments and results.

A.1 Supplementary Figures

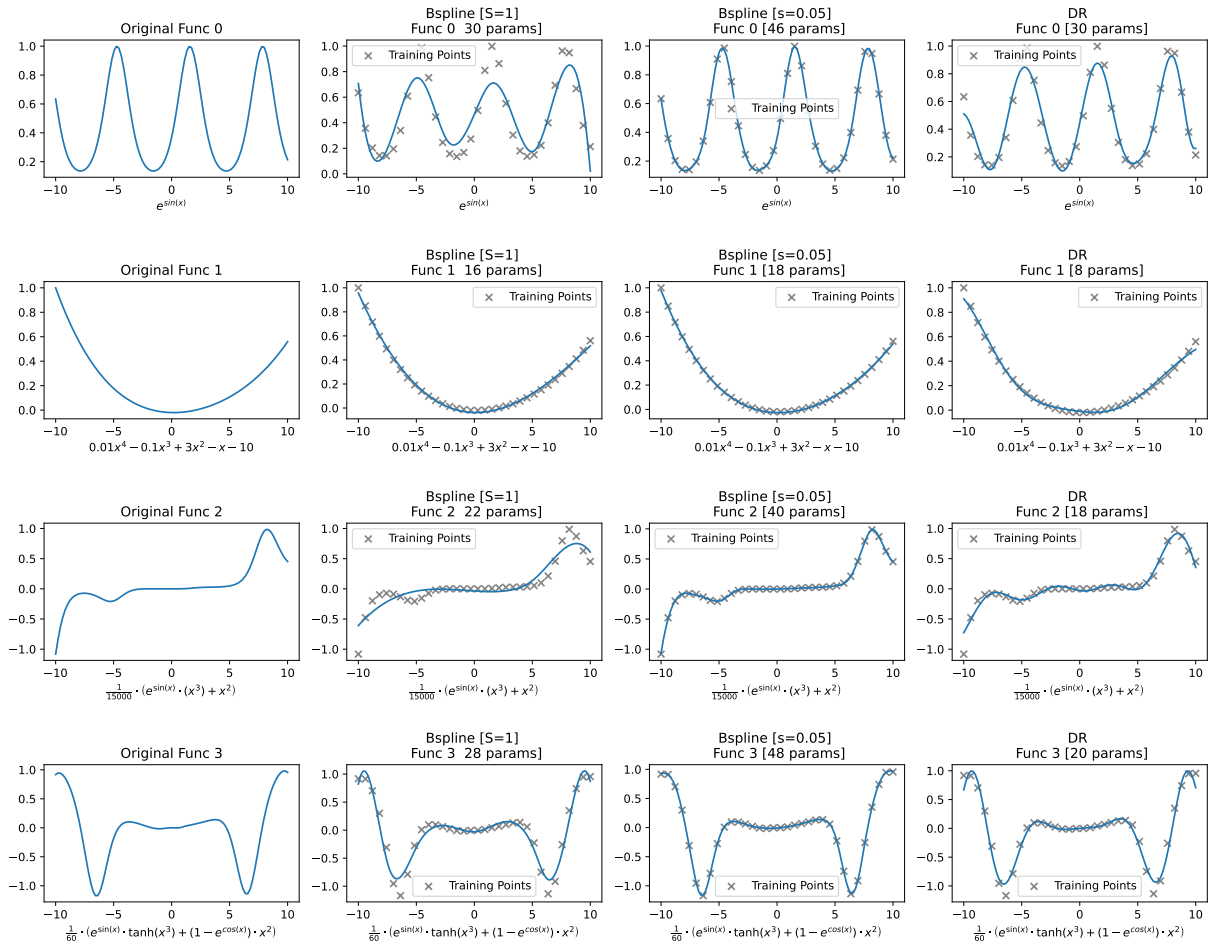


Figure A.1: Expanded DR vs B-Spline Comparisons

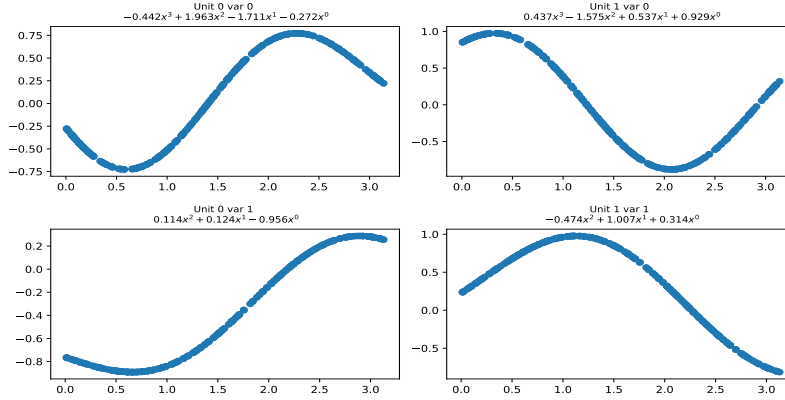


Figure A.2: The functions learned by the QuIRK model described in Section 4.4 and the polynomials for the functions

A.2 Supplementary Tables

Table A.1: Full Comparison between all QuIRK and Classical KAN variants

Equation	QuIRK (Ours)		QuIRK Pruned		Classical KAN		Classical KAN Pruned	
	Loss	# Params						
I.6.2	1.40×10^{-3}	36	2.95×10^{-2}	24	3.90×10^{-1}	136	1.51×10^0	56
I.6.2b	2.64×10^{-3}	72	2.01×10^{-2}	32	3.68×10^{-1}	244	6.91×10^{-1}	72
I.9.18	9.00×10^{-3}	234	1.06×10^{-2}	120	4.99×10^{-1}	736	1.65×10^0	120
I.12.11	1.04×10^{-2}	48	5.64×10^{-2}	24	9.90×10^{-4}	136	1.58×10^{-1}	56
I.13.12	4.20×10^{-3}	36	7.67×10^{-2}	24	2.54×10^1	136	2.50×10^1	56
I.15.3x	1.30×10^{-2}	36	1.84×10^{-2}	24	5.14×10^{-1}	80	6.48×10^{-1}	56
I.16.6	1.38×10^{-2}	36	6.50×10^{-2}	24	3.34×10^{-2}	136	4.40×10^{-1}	56
I.18.4	8.00×10^{-3}	36	5.17×10^{-2}	24	1.31×10^1	136	4.87×10^1	56
I.26.2	7.07×10^{-2}	60	2.81×10^{-2}	40	4.20×10^{-3}	136	1.71×10^{-1}	56
I.27.6	2.31×10^{-2}	54	2.37×10^{-2}	36	3.25×10^{-1}	136	1.28×10^0	56
I.29.16	1.24×10^{-2}	51	8.99×10^{-2}	35	7.81×10^{-3}	391	1.99×10^{-1}	72
I.30.3	4.79×10^{-2}	43	7.05×10^{-2}	27	4.13×10^{-3}	136	4.43×10^{-3}	56
I.30.5	5.53×10^{-2}	82	6.37×10^{-2}	40	3.31×10^{-1}	156	4.92×10^{-1}	56
I.37.4	7.50×10^{-2}	76	1.56×10^{-1}	40	9.08×10^{-3}	136	4.82×10^{-2}	56
I.40.1	8.73×10^{-2}	68	5.85×10^{-2}	40	3.65×10^{-2}	136	3.88×10^{-1}	56
I.44.4	3.74×10^{-2}	48	3.61×10^{-2}	24	4.63×10^{-2}	156	6.26×10^{-1}	56
I.50.26	2.40×10^{-2}	54	4.86×10^{-2}	36	4.10×10^{-4}	192	5.19×10^{-2}	56
II.2.42	9.98×10^{-2}	36	6.49×10^{-2}	24	3.90×10^{-4}	136	3.33×10^{-1}	56
II.6.15a	2.04×10^{-2}	76	4.60×10^{-2}	52	2.00×10^{-3}	202	1.31×10^{-2}	72
II.11.7	8.55×10^{-2}	72	6.68×10^{-2}	48	8.21×10^{-3}	272	1.98×10^{-1}	84
II.11.27	4.92×10^{-2}	36	5.93×10^{-2}	24	4.48×10^{-2}	136	2.20×10^{-1}	56
II.35.18	5.24×10^{-2}	20	6.59×10^{-2}	14	1.26×10^1	136	1.17×10^1	56
II.36.38	2.72×10^{-3}	51	1.32×10^{-2}	35	5.40×10^{-4}	244	3.35×10^{-1}	72
II.38.3	6.10×10^{-3}	72	4.79×10^{-2}	32	2.54×10^1	80	2.33×10^1	56
III.9.52	3.06×10^{-2}	102	4.97×10^{-2}	62	2.20×10^{-4}	342	8.93×10^{-2}	72
III.10.19	1.41×10^{-2}	58	6.55×10^{-2}	40	3.00×10^{-5}	80	3.64×10^{-3}	56
III.17.37	1.11×10^{-3}	76	7.52×10^{-2}	52	3.43×10^{-3}	244	2.81×10^{-1}	72

Table A.2: Full Comparison between all DR-KAN QuIRK variants and Vanilla DR Models

Equation	QuIRK (Ours) Pruned		Vanilla DR	
	Loss	# Params	Loss	# Params
I.6.2	2.95×10^{-2}	24	1.46×10^{-1}	30
I.6.2b	2.01×10^{-2}	32	6.65×10^{-1}	30
I.9.18	1.06×10^{-2}	120	2.07×10^1	30
I.12.11	5.64×10^{-2}	24	1.48×10^{-1}	30
I.13.12	7.67×10^{-2}	24	3.13×10^1	30
I.15.3x	1.84×10^{-2}	24	3.64×10^0	30
I.16.6	6.50×10^{-2}	24	2.89×10^{-1}	30
I.18.4	5.17×10^{-2}	24	2.83×10^{-1}	30
I.26.2	2.81×10^{-2}	40	1.67×10^{-1}	30
I.27.6	2.37×10^{-2}	36	6.52×10^{-2}	30
I.29.16	8.99×10^{-2}	35	8.03×10^{-1}	30
I.30.3	7.05×10^{-2}	27	1.01×10^0	30
I.30.5	6.37×10^{-2}	40	2.88×10^{-1}	30
I.37.4	1.56×10^{-1}	40	3.36×10^{-1}	30
I.40.1	5.85×10^{-2}	40	1.38×10^{-1}	30
I.44.4	3.61×10^{-2}	24	2.49×10^0	30
I.50.26	4.86×10^{-2}	36	3.57×10^{-1}	30
II.2.42	6.49×10^{-2}	24	1.68×10^0	30
II.6.15a	4.60×10^{-2}	52	3.89×10^0	30
II.11.7	6.68×10^{-2}	48	3.66×10^0	30
II.11.27	5.93×10^{-2}	24	2.56×10^2	30
II.35.18	6.59×10^{-2}	14	2.09×10^{-1}	30
II.36.38	6.32×10^{-2}	35	2.36×10^0	30
II.38.3	4.79×10^{-2}	32	1.35×10^2	30
III.9.52	4.97×10^{-2}	62	9.12×10^{-2}	30
III.10.19	6.55×10^{-2}	40	5.34×10^{-1}	30
III.17.37	7.52×10^{-2}	52	3.35×10^0	30

Table A.3: Performance comparison of equations with DR-KAN, KAN and MLP models. Losses in RMSE. Results of KAN and MLP (Best Accuracy) directly from KAN paper. Our Shape is [2,1] with DR layers [3,3] for 43 params and [4,3] for 51 params.

Equation	DR-KAN	# Params	Min KAN	Min KAN	Best KAN	Best KAN	MLP
JacobElliptic	8.78×10^{-3}	55	[2,2,1]	7.29×10^{-3}	[2,3,2,1,1,1]	1.33×10^{-4}	6.48×10^{-4}
EllipticInt1	2.79×10^{-3}	43	[2,2,1]	1.00×10^{-3}	[2,2,1,1,1]	1.24×10^{-4}	5.52×10^{-4}
EllipticInt2	1.26×10^{-2}	43	[2,2,1,1]	8.36×10^{-5}	[2,2,1,1]	8.26×10^{-5}	3.04×10^{-4}
BesselJ	3.95×10^{-2}	43	[2,2,1]	4.93×10^{-3}	[2,3,1,1,1]	1.64×10^{-3}	5.52×10^{-3}
BesselY	2.59×10^{-2}	43	[2,3,1]	1.89×10^{-3}	[2,2,2,1]	1.49×10^{-3}	3.45×10^{-4}
BesselK	2.48×10^{-2}	43	[2,1,1]	4.89×10^{-3}	[2,2,1]	2.52×10^{-5}	1.67×10^{-4}
BesselI	4.12×10^{-3}	43	[2,4,3,2,1,1]	9.28×10^{-3}	[2,4,3,2,1,1]	9.28×10^{-3}	1.07×10^{-2}
Legendre0	2.66×10^{-3}	43	[2,2,1]	5.25×10^{-5}	[2,2,1]	5.25×10^{-5}	1.74×10^{-2}
Legendre1	7.22×10^{-3}	51	[2,4,1]	6.90×10^{-4}	[2,4,1]	6.90×10^{-4}	1.50×10^{-3}
Legendre2	8.66×10^{-3}	43	[2,2,1]	4.88×10^{-3}	[2,3,2,1]	2.26×10^{-3}	9.43×10^{-4}
SH01	5.16×10^{-3}	43	[2,1,1]	2.21×10^{-7}	[2,1,1]	2.21×10^{-7}	1.25×10^{-6}
SH11	2.84×10^{-2}	43	[2,2,1]	7.86×10^{-4}	[2,3,2,1]	1.22×10^{-4}	6.70×10^{-4}
SH02	8.29×10^{-3}	43	[2,1,1]	1.95×10^{-7}	[2,1,1]	1.95×10^{-7}	2.85×10^{-6}
SH12	2.09×10^{-2}	43	[2,2,1]	4.70×10^{-4}	[2,2,1,1]	1.50×10^{-5}	1.84×10^{-3}
SH22	6.44×10^{-2}	43	[2,2,1]	1.12×10^{-3}	[2,2,3,2,1]	9.45×10^{-5}	6.21×10^{-4}

Table A.4: RMSE Loss for MLPs and KAN on the Feynman dataset when the outputs are constrained to $[-1,1]$.

Equation	MLPs				DR-KAN	
	Less Params		Sufficient Params		Loss (Ours)	# Params
	Loss	# Params	Loss	# Params		
1.6.2	5.69×10^{-3}	133	1.43×10^{-3}	2305	1.40×10^{-3}	36
1.6.2b	4.61×10^{-3}	57	6.16×10^{-3}	253	2.64×10^{-3}	72
1.9.18	3.42×10^{-3}	133	3.28×10^{-4}	2305	9.00×10^{-3}	234
1.12.11	3.33×10^{-3}	57	3.96×10^{-4}	565	1.40×10^{-2}	48
1.13.12	2.21×10^{-3}	133	2.36×10^{-4}	565	4.20×10^{-3}	36
1.15.3x	9.35×10^{-3}	133	4.79×10^{-4}	565	1.30×10^{-2}	36
1.16.6	1.61×10^{-2}	133	2.60×10^{-3}	565	1.38×10^{-2}	36
1.18.4	6.07×10^{-3}	133	7.59×10^{-4}	565	8.00×10^{-3}	36
1.26.2	4.02×10^{-3}	133	1.66×10^{-3}	2305	7.07×10^{-3}	60
1.29.16	2.47×10^{-3}	133	1.02×10^{-3}	2305	2.31×10^{-2}	54
1.30.2	4.00×10^{-3}	133	1.01×10^{-3}	565	1.24×10^{-2}	51
1.37.6	8.97×10^{-2}	133	2.19×10^{-3}	2305	4.79×10^{-3}	50
1.44.4	3.10×10^{-3}	133	4.18×10^{-4}	2305	5.53×10^{-3}	82
1.44.6	3.29×10^{-3}	133	3.12×10^{-4}	565	7.50×10^{-3}	76
II.4.2	5.62×10^{-4}	133	1.02×10^{-4}	565	8.73×10^{-3}	60
II.6.15a	1.01×10^{-3}	133	9.30×10^{-5}	2305	5.00×10^{-3}	48
II.11.7	9.47×10^{-4}	133	4.55×10^{-4}	2305	2.40×10^{-3}	54
II.15.18	1.01×10^{-3}	133	3.93×10^{-4}	565	9.98×10^{-3}	36
II.35.36a	1.24×10^{-3}	133	8.30×10^{-5}	565	2.04×10^{-3}	48
II.38.7	2.15×10^{-3}	133	2.33×10^{-4}	565	8.55×10^{-3}	72
II.9.52	2.65×10^{-3}	133	1.43×10^{-4}	565	4.92×10^{-3}	36
II.10.19	1.99×10^{-3}	133	3.00×10^{-4}	2305	5.24×10^{-3}	20
III.17.37	1.63×10^{-3}	133	1.52×10^{-4}	2305	2.72×10^{-3}	36